Dalton Transactions

ROYAL SOCIETY OF CHEMISTRY

PAPER

View Article Online
View Journal | View Issue



Cite this: *Dalton Trans.*, 2024, **53**, 18484



# A serendipitous crossed aldol reaction in the ligand periphery of a Ru(II) polypyridyl complex in silica bed: prospects for delivering anticancer agents for photoactivated chemotherapy†

Ramranjan Mishra,‡[a] Pritha Chatterjee, ‡[a] Ray J. Butcher [b] and Ashis K. Patra *[a]

Received 16th August 2024,
Accepted 18th October 2024

DOI: 10.1039/d4dt02337d

rsc.li/dalton

The localized drug action in tumors to overcome the side effects of chemotherapy has become an impetus for the development of photoactivated chemotherapy (PACT). As potential PACT agents, ruthenium(II) polypyridyl complexes have emerged as efficient photocages for anticancer agents. Bioactive molecules possessing functional groups such as nitrile, thioether, pyridine, imidazole, *etc*. are often directly attached to the primary coordination sphere of Ru(II) polypyridyl complexes for this purpose. Herein, we propose an alternative design strategy to attach potential anticancer agents lacking these functional groups with Ru(II) polypyridyl complexes through a pyridyl linker moiety. The proposition is, however, a thoughtful extrapolation of a serendipitous crossed aldol reaction that took place between the Ru(II)-coordinated 4-Pyridinecarboxaldehyde (4-PyCHO) and acetone, discovered while the Ru(II)-complex $[Ru(ttp)(dppz)(4\text{-PyCHO})]^{2+}$ {[**1**]} [ttp = *p*-tolyl terpyridine, dppz = dipyrido[3,2-*a*:2′,3′-*c*]phenazine, 4-PyCHO = 4-Pyridinecarboxaldehyde] was being purified by silica gel column chromatography with acetone/water/saturated aqueous $KNO_3$ solution as the eluent. The resultant pure aldol product $[Ru(ttp)(dppz)(4\text{-PyCHAc})]^{2+}$ {[**1-Ac**]} [4-PyCHAc = aldol modified 4-Pyridinecarboxaldehyde, *i.e.*, 4-hydroxy-4-(pyridin-4-yl)butan-2-one)], was unambiguously characterized by a variety of spectroscopic techniques and X-ray crystallography. Furthermore, a $^1$H NMR study after 470 nm light irradiation and subsequent ESI-MS analysis revealed that 4-PyCHO could be photo-released from [**1-Ac**] as its *in situ* generated aldol adduct 4-PyCHAc. Therefore, this finding serves as a proof-of-concept that provides a simpler alternative design strategy for appending cancer-selective agents having carbonyl groups with α-hydrogens to ruthenium(II) polypyridyl complexes and their photorelease for selective and targeted anticancer chemotherapy.

## Introduction

The working principle of photoactivated chemotherapy (PACT) relies on the locally resurged biological activity of the constituent species of a judiciously designed inert 'prodrug' species with visible to NIR light as the stimulus within the phototherapeutic window.[1–3] The scope of exploring ruthenium(II) polypyridyl complexes as optimal PACT agents is phenomenal, as this class of molecules allow wide-ranging modulation of photophysical properties and ligand-exchange kinetics depending on the ligand framework surrounding the metal center.[1,2,4] The contemporary research in this direction encompasses the caging of several thioether, nitrile, pyridine, amine, imidazole, and diazine functional group-based anticancer agents with ruthenium(II) polypyridyl complexes for more selective and effective delivery of these drugs or anticancer agents (Fig. 1).[5–29] The molecules with these previously mentioned functional groups are directly covalently linked with the Ru(II) center and subsequently photo-ejected as a result of the population of a dissociative $^3$MC (dσ*) state from the photogenerated $^3$MLCT state.[1–4] However, many anticancer agents or drugs lacking these functional groups are attached to Ru(II) polypyridyls by their structural modification through covalent linkages with thioethers, pyridines, triazolyl moieties, *etc*. to reduce their systemic toxicity and/or controlled delivery. For example, Huisman *et al.* proposed the caging of an epoxy suc-

[a]*Department of Chemistry, Indian Institute of Technology Kanpur, Kanpur 208016, Uttar Pradesh, India. E-mail: akpatra@iitk.ac.in*
[b]*Department of Chemistry, Howard University, Washington, DC 20059, USA*

†Electronic supplementary information (ESI) available. CCDC 2377849. For ESI and crystallographic data in CIF or other electronic format see DOI: https://doi.org/10.1039/d4dt02337d

‡These authors contributed equally to this work.

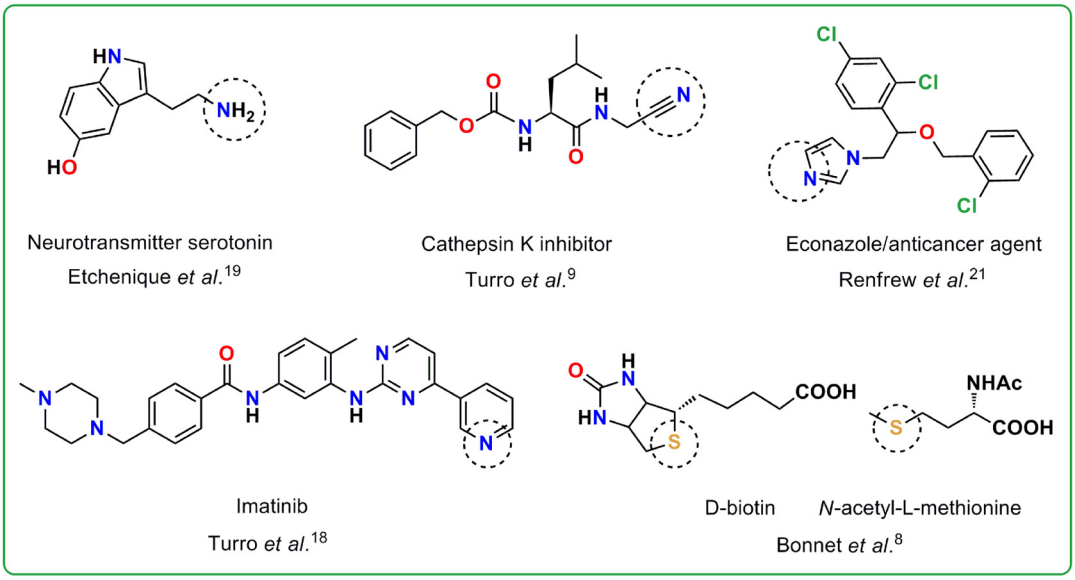


**Fig. 1** Examples of previously reported amine, nitrile, imidazole, pyridine and thioether-based anticancer agents/bio-active molecules directly attached to the Ru(II) center in Ru(II) polypyridyl complexes. The binding sites with Ru(II) are marked as dotted circles.

cinyl-based cysteine cathepsin inhibitor by replacing the phenyl side arm of the CLIK-148 inhibitor and CLIK-181 with pyridine ring for reversible binding with Ru(II), which would uncage the inhibitors upon light irradiation.[30] This strategy, as established by the authors, enabled kinetic control over the irreversible inhibition of the cysteine protease-based enzyme cathepsin L. Apart from that, Kodanko and co-workers in their recent works have reported the attachment of cathepsin B inhibitors to Ru(II) polypyridyl complexes through pyridyl/triazolyl-based linkers and their subsequent photorelease.[31,32] In these reports, cathepsin B inhibitors were linked with pyridine/triazolyl derivatives through covalent linkages and then the pyridyl/triazolyl moiety was utilized for their attachment and subsequent photorelease from the Ru(II) polypyridyl core. Moreover, Bonnet *et al.* also attached one membrane intercalator 3α,5β-cholestanol to Ru(II) polypyridyl complexes by forming a covalent linkage in between the membrane intercalator and a thioether-based monodentate ligand.[5]

Herein, we propose a simple, synthetically straightforward method to append bioactive carbonyl compounds having a carbonyl moiety with α-hydrogens such as 3-bromo pyruvic acid[33–35] by functionalization of a Ru(II)-coordinated pyridine derived ligand 4-Pyridinecarboxaldehyde. The spatiotemporal control over the drug's activity, offered by photoinduced ligand release from Ru(II) polypyridyl complexes, could potentially be achieved for anticancer agents like 3-bromo pyruvic acid in this manner. The overall narrative presented in this work, however, is a thoughtfully proposed augmentation of a serendipitous aldol reaction between acetone and 4-Pyridinecarboxaldehyde directly coordinated to Ru(II) in $[Ru(ttp)(dppz)(4\text{-PyCHO})]^{2+}$ {[**1**]} [here ttp = *p*-tolyl terpyridine, dppz = dipyrido[3,2-*a*:2′,3′-*c*]phenazine, 4-PyCHO = 4-Pyridinecarboxaldehyde], while it was being purified with acetone/water/saturated aqueous $KNO_3$ solution in silica to result in the aldol product $[Ru(ttp)(dppz)(4\text{-PyCHAc})]^{2+}$ (4-PyCHAc = aldol modified 4-Pyridinecarboxaldehyde, *i.e.*, 4-hydroxy-4-(pyridin-4-yl)butan-2-one) {[**1-Ac**]} (*vide* Scheme 1 for the chemical structures).

Although not within the scope of this work, the aldehyde (–CHO) functional group in 4-PyCHO can be intelligently exploited as a generic synthon to attach bioactive molecules in the second coordination sphere of Ru(II) polypyridyl complexes. In addition, conjugating cancer-targeting molecules with Ru(II) polypyridyl complexes is feasible for the target-specific delivery of Ru(II)-prodrugs *via* various other well-known reactions of aldehyde groups, *viz.* Knoevenagel condensation, Wittig reaction, Baylis–Hillman reaction, Schiff base reaction, *etc.*[36–39]

The present work describes the synthesis and characterization of [**1**] and [**1-Ac**] by various spectroscopic techniques and X-ray crystallography. The blue-LED induced release of 4-PyCHAc from [**1-Ac**] in its aldol form was monitored by a time-dependent $^1$H NMR study and subsequent ESI-MS-based speciation of the photoproducts was carried out. The work also highlights the limitations and lays the foundation towards future scope for feasible designs that can more efficiently and reversibly attach bioactive molecules to formulate Ru(II)-prodrugs.

## Results and discussion

### Synthesis of {[1]} and {[1-Ac]}

First, the intermediate $[Ru(ttp)(dppz)(H_2O)](PF_6)_2$ was synthesized in a sequence of steps as reported previously.[40–42] Consequently, refluxing $[Ru(ttp)(dppz)(H_2O)](PF_6)_2$ in the pres-

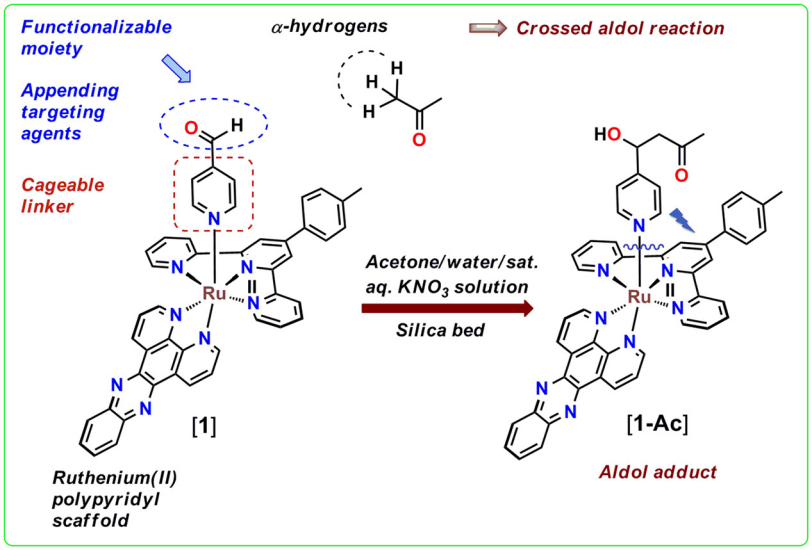


**Scheme 1** Simple design strategy for the attachment of anticancer agents through a pyridine-based photocageable linker to Ru(II) polypyridyl complexes *via* functionalization of the –CHO moiety present in the monodentate ligand.

ence of 4-Pyridinecarboxaldehyde in acetone results in the final product [Ru(ttp)(dppz)(4-PyCHO)]$(PF_6)_2$ as evidenced by both ESI-MS in methanol and $^1$H NMR in DMSO-$d_6$ (Scheme 2). However, the product isolated as a $PF_6^-$ salt was impure and the presence of a Ru(II)-based impurity was observable from the NMR spectrum. Hence, the impure 4-Pyridinecarboxaldehyde-based complex [Ru(ttp)(dppz)(4-PyCHO)]$(PF_6)_2$ [**1**] was subjected to purification by using a silica gel column. During the elution from the column, the last orange-red band eluted with acetone/water/saturated aqueous $KNO_3$ solution (85 : 5 : 0.5) was collected and the subsequent evaporation of the solvent yielded a red powder. The purity of this band was established by a single spot in TLC. The characterization of the pure product by several spectral techniques and X-ray crystallography elicits a new outlook, and therefore the characterization of the product is thoroughly discussed and analyzed in detail in the subsequent subsections.

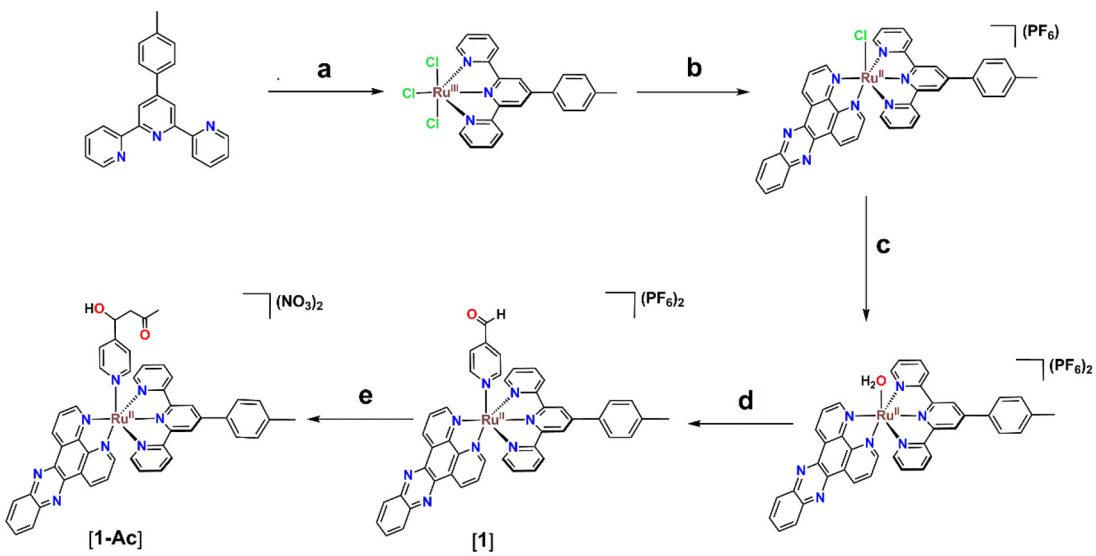


**Scheme 2** Synthetic scheme showing the synthesis of [Ru(ttp)(dppz)(4-PyCHO)]$(PF_6)_2$ [**1**] and purification by column chromatography, which led to the formation of [**1-Ac**]. (a) $RuCl_3{\cdot}3H_2O$, reflux in EtOH for 4 h. (b) dppz, $NEt_3$, LiCl in 3 : 1 EtOH/$H_2O$, $N_2$ atmosphere, and saturated aqueous $KPF_6$ solution. (c) $AgNO_3$, stirring at 50 °C in 2 : 1 acetone/water for 16 h under a $N_2$ atmosphere, and saturated aqueous $KPF_6$ solution. (d) 4-Pyridinecarboxaldehyde, reflux for 24 h in acetone under a $N_2$ atmosphere. (e) Silica bed, acetone/water/saturated aqueous $KNO_3$ solution (85 : 5 : 0.5).

### Solution-state characterization of the product from the silica column chromatography

At first, the identity of the product was examined by ESI-MS spectrometry, and surprisingly a peak with $m/z$ = 934.20 (Fig. S1a, ESI†) was observed with a matching isotopic pattern of ruthenium instead of the peak at 991.16 {$[M - PF_6^-]^+$} observed for [**1**](PF$_6$)$_2$ (Fig. S1b, ESI†). The molecular ion peak with $m/z$ at 934.20 is ascribed to the aldol adduct [**1-Ac**] (*vide* Scheme 1 for the chemical structure). Hence, this change in the mass spectra before and after column chromatography indicates a possible structural modification in the silica gel column bed. Therefore, the $^1$H NMR spectrum of the product was analyzed and compared with that of [**1**] in DMSO-$d_6$. The $^1$H NMR spectrum of the product as shown in Fig. 2 was very different from that of [**1**]. In particular, the aliphatic region clearly illustrates the appearance of some new peaks at 5.69 ppm (doublet), 4.98 ppm (doublet of triplets), and at 2.71 and 2.67 ppm (ABX second order splitting pattern), which were absent in the $^1$H NMR spectrum of [**1**]. Apart from that, a singlet at 10.02 ppm observed for the –C**H**O proton of the bound 4-Pyridinecarboxaldehyde in [**1**] was not observed in the product eluted from the column. Moreover, the most downfield shifted doublet of [**1**] observed at 9.96 ppm shifted slightly upfield in the product to 9.89 ppm. The full $^1$H NMR spectrum of the product with chemical shift values and integrations for each peak is shown in Fig. S2, ESI.† The presence of a total of twenty-eight aromatic protons obtained from $^1$H NMR integration is compatible with the structure of [**1-Ac**] and only one singlet at 9.31 ppm integrated for two protons also indicates the presence of an analytically pure ruthenium(II) compound with $C_s$ symmetry. At this point, for exact elucidation of the structure of the product as [**1-Ac**], the analysis of the aliphatic peaks in the $^1$H NMR spectrum would be most reliable. The doublet at 5.69 ppm correlates with the doublet of the triplet peak at 4.98 ppm according to the COSY spectrum in DMSO-$d_6$ (Fig. 3). This doublet at 5.69 ppm is assigned to the –O**H** proton, which is coupled with the H$_X$ proton ($\delta$ = 4.98 ppm), as illustrated in the expanded aliphatic region of the NMR spectrum in Fig. 3. In contrast, the H$_X$ proton couples not only with the peak at 5.69 ppm, but also with the signals at 2.71 and 2.67 ppm (H$_A$ and H$_B$) (Fig. 3). Upon careful examination of the structure of the product [**1-Ac**], it is apparent that even though the overall complex has time-averaged $C_s$ symmetry due to conformational mobility in the solution as suggested by $^1$H NMR, the methylene protons (H$_A$ and H$_B$) are diastereotopic and should be in slightly different chemical environments. However, due to a very high coupling constant ($J_{AB}$ = 16 Hz) and a small difference in their chemical shifts ($\Delta\nu$), the two signals which should otherwise appear as two individual doublets of doublets integrated for one proton each were observed as a complex second-order ABX pattern integrated for two hydrogens ($\Delta\nu/J$ = 1.25) (Fig. S3, ESI†). The coupling constant values and the chemical shifts of the AB part of the ABX pattern were calculated by considering and identifying the two AB quartets and obtaining the $J_{AB}$ value first and then the $J_{AX}$ (5.5 Hz) and $J_{BX}$ (7.5 Hz) values were calculated. The analysis of the X part of the ABX pattern was rather straightforward also because of the very high chemical shift difference from the AB part. However, one more degree of

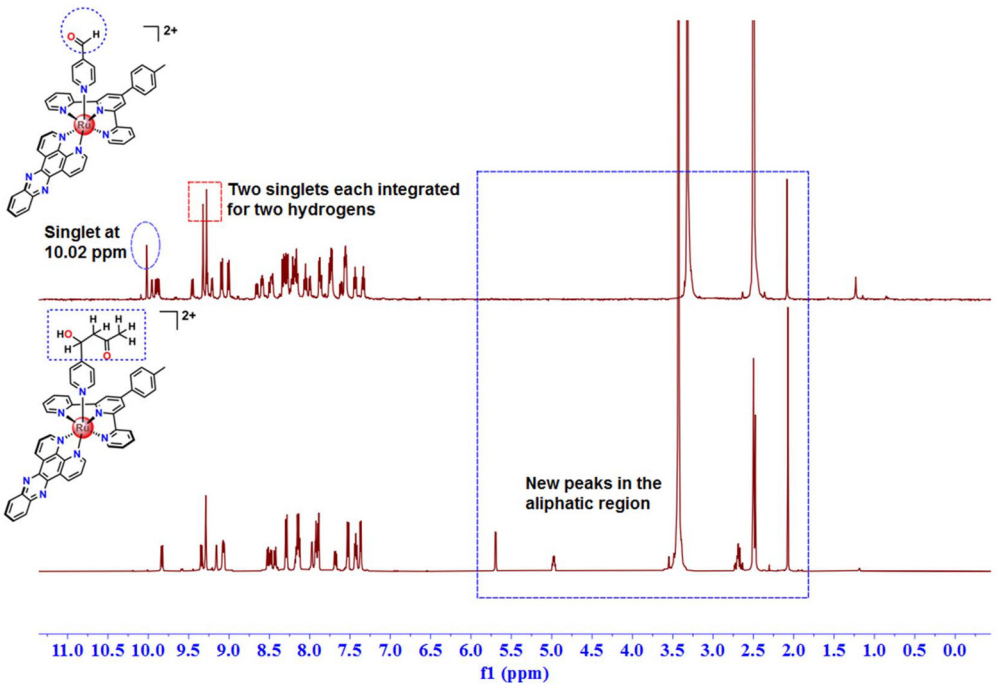


**Fig. 2** $^1$H NMR of the aldol product, [Ru(ttp)(dppz)(4-PyCHAc)]$^{2+}${[**1-Ac**]}, in comparison with [Ru(ttp)(dppz)(4-PyCHO)](PF$_6$)$_2$ [**1**] in DMSO-$d_6$.

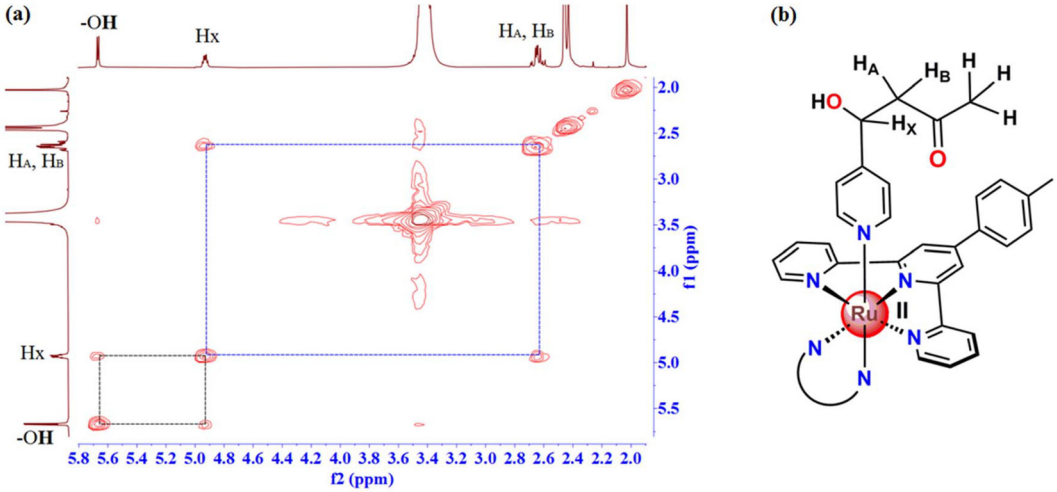


**Fig. 3** (a) $^{1}$H–$^{1}$H COSY in DMSO-$d_6$ suggesting the correlation between the aliphatic protons of [**1-Ac**]. (b) Chemical structure of [**1-Ac**] highlighting the selected protons that correlate in $^{1}$H–$^{1}$H COSY.

complexity is added there due to further coupling with the –O**H** proton, which is generally observable in solvents like DMSO-$d_6$. Therefore, the X part, which in the absence of coupling with the –O**H** proton would have appeared as a doublet of doublet or sometimes a triplet, was observed as a doublet of triplets. This complexity was disentangled to some extent by recording the $^{1}$H NMR spectrum of [**1-Ac**] in a solvent like $CD_3OD$, where due to deuterium exchange, the coupling of $H_X$ with the –O**H** proton could be eliminated (Fig. S4, ESI†). As expected in the $^{1}$H NMR spectrum in $CD_3OD$, apart from the absence of the signal for the –O**H** proton, the $H_X$ proton was observed as a doublet of doublet at 5.11 ppm, which is consistent with its position being adjacent to the diastereotopic methylene protons. The chemical shift of the $H_X$ proton in both DMSO-$d_6$ and $CD_3OD$ is also broadly in line with that expected for a –C**H**OH proton. Moreover, the A and B protons were also observed in the complex ABX pattern, just like in DMSO-$d_6$. Apart from that, a singlet at 2.08 ppm integrated for three protons in DMSO-$d_6$ is also consistent with the –C**H**$_3$ protons adjacent to the –CO group. To corroborate the identity of the product eluted from the column as [**1-Ac**], further characterization with $^{13}$C NMR in DMSO-$d_6$ was adopted. The $^{13}$C NMR spectra show four aliphatic peaks at 67.2, 51.6, 30.7 and 21.5 ppm (Fig. S5, ESI†). The $^{13}$C signal at 21.5 ppm is consistent with –Ph**Me** carbon of the *p*-tolyl ring of the tridentate ligand and the presence of an aliphatic signal at 30.7 ppm, and the most downfield shifted peak at 206.5 ppm indicates the presence of a –COCH$_3$ moiety in the structure. The peak at 206.5 ppm can be ascribed to the –**C**O carbon of the –COCH$_3$ moiety and the corresponding aliphatic signal appears at 30.7 ppm for the –**C**H$_3$ carbon. Furthermore, the peaks at 67.2 and 51.6 ppm can be attributed to the –**C**HOH carbon and the methylene carbon, respectively, from their chemical environment. These assignments were further consolidated by the $^{1}$H–$^{13}$C HSQC spectra in DMSO-$d_6$ (Fig. S6, ESI†), where the $^{13}$C signals at 67.2 ppm and 30.7 ppm were found to be interacting with the peaks at 4.98 ppm and 2.08 ppm in $^{1}$H NMR, respectively. Moreover, the $^{13}$C peak at 51.6 ppm showed a correlation with the $^{1}$H NMR peaks at 2.71 and 2.67 ppm assigned to the diastereotopic methylene protons (only twelve lines were observed in the ABX pattern). Therefore, collectively the ESI-MS and $^{1}$H NMR-based characterization data provide enough evidence for the initiation of a crossed aldol reaction between the coordinated 4-pyridine carboxaldehyde and acetone in the silica bed during the purification of the crude 4-Pyridinecarboxaldehyde-based Ru(II) complex [**1**]. Also, it is worth mentioning that the spectroscopic evidence in the solution state suggested that the product did not undergo any subsequent condensation. The aldol adduct [**1-Ac**] was further characterized in the solution state by UV-vis absorption spectroscopy and cyclic voltammetry. In the UV-vis spectrum (Fig. S7a, ESI†), one broad peak at 495 nm was observed in DMSO ascribed to the metal-to-ligand charge transfer band ($^{1}$MLCT).[40,41] When this MLCT band was compared with the structurally similar compounds reported in the literature, we found a slight red-shift in the MLCT band of [**1-Ac**] probably due to the contribution of the dppz ligand to the LUMO.[40] Cyclic voltammetry of [**1-Ac**] in MeCN reveals only a single oxidation process attributed to the $Ru^{II/III}$ couple around 0.88 V *vs.* $Fc/Fc^{+}$ with $\Delta E$ = 77 mV and $i_{pc}/i_{pa}$ = 0.4 (Fig. S7b, ESI†). The oxidation peak potential is comparable with the previous literature reporting $[Ru(tpy)(dppz)(py\text{-}R)]^{2+}$ systems with different pyridine derivatives as monodentate ligands.[41] The complex was non-luminescent at room temperature when excited at the MLCT band.

## Solid state characterization of [1-Ac] using X-ray crystallography

The molecular structure of the crossed aldol product $[Ru(ttp)(dppz)(4\text{-}PyCHAc)]^{2+}$ [**1-Ac**] was unequivocally confirmed

 

through single crystal X-ray diffraction studies. Good quality crystals were obtained by slow diffusion of $Et_2O$ into the solution of [**1-Ac**] in MeCN. The compound crystallized in the $P2_1/c$ space group of the monoclinic crystallographic system. The ORTEP view of [**1-Ac**] is shown in Fig. 4 and the important bond distances and bond angles concerning the atoms directly attached to Ru(II) are represented in Tables S1 and S2 in the ESI.† The crystal structure reveals an octahedral geometry of the [Ru(N3)(N2)(N)] type, where the three equatorial sites were occupied by the three N atoms (N1, N2 and N3) of the *p*-tolyl terpyridine ligand (ttp) and the remaining site by one N atom (N4) of the bidentate dppz ligand. The Ru1–N5 and Ru1–N6 axial bond lengths are in good agreement with the structurally similar compounds reported in the literature.[40,41] As can be seen in Tables S1 and S2,† the slight deviation from a perfect octahedral geometry originates from the shorter bite angles provided by the ttp and dppz ligands. On the other hand, the angle between the mean plane containing the dppz ligand and the equatorial plane encompassing the tridentate ttp ligand is ~88°, suggesting the inability of the dppz ligand to further distort the geometry. Moreover, the crystal structure clearly reveals the identity of the compound as a crossed aldol adduct formed due to the reaction between the coordinated 4-Pyridinecarboxaldehyde and acetone. The aldol-modified ligand 4-PyCHAc was axially bound to Ru(II) *via* a pyridine-N atom (N6). The distance between the *in situ* formed C–C bond in the silica bed, *i.e.* C44–C45 in 4-PyCHAc, was found to be ~1.44 Å, which is slightly shorter than that expected for the C–C single bond, though much longer than a typical C=C double bond. The oxygen atom of the –C–OH bond was disordered over two positions and therefore was split into two parts each with 0.5 site occupancy. In the extended lattice structure, the –C–OH moiety of the aldol product and co-crystallized $H_2O$ molecules were found to have intermolecular hydrogen bonding interactions with the nitrate counter ions. Surprisingly, in the asymmetric unit of the crystal structure, there were three nitrate ($NO_3^-$) counter anions, which at first glance seem dubious, as all the other spectroscopic techniques such as ESI-MS, $^1$H NMR, and EPR suggested the presence of a Ru(II) species. Therefore, at first, the probability of the nitrates being positioned in the special positions with possible fractional occupancy in the unit cell was scrutinized.

However, when that probability was completely ruled out, a much closer look into the electron density map suggested that one co-crystallized water molecule was actually $H_3O^+$ and that accounts for the three nitrate counter ions in the asymmetric unit. This is not unlikely because we used saturated aqueous $KNO_3$ solution for the purification process in the silica gel column. Therefore, we presume this is the probable reason for the presence of $H_3O^+$ and $NO_3^-$ in the crystal structure, which we were unable to identify using any other spectroscopic techniques. Moreover, in the presence of a strong acid, the product obtained was in the form of an aldol adduct [**1-Ac**], as suggested by all the solution-state characterization techniques and determination of the molecular structure. Therefore, the role of the silica bed and the saturated aqueous $KNO_3$ solution in facilitating the aldol reaction can be conjectured. The crystallographic refinement details are given in Table S3 in the ESI.†

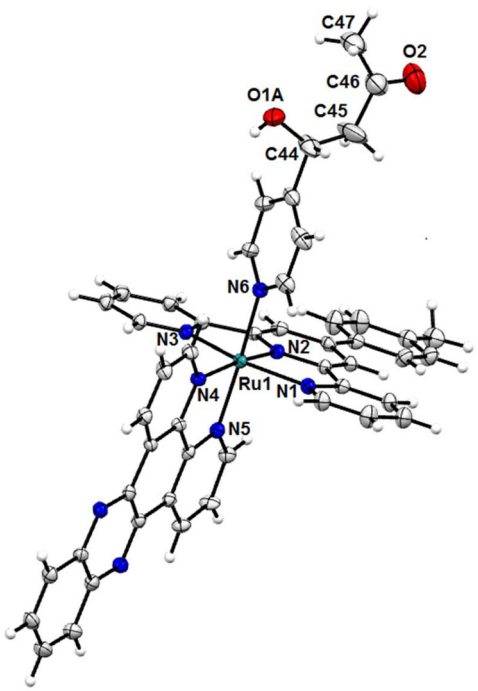


**Fig. 4** ORTEP diagram of $[Ru(ttp)(dppz)(4\text{-}PyCHAc)]^{2+}$ [**1-Ac**] represented with 50% probability. The $NO_3^-$ counter ions and the co-crystallized solvents were omitted for clarity.

### Photorelease of 4-PyCHAc from $[Ru(ttp)(dppz)(4\text{-}PyCHAc)]^{2+}$ {[**1-Ac**]}

To monitor the photorelease of the ligand and subsequent speciation, at first, $[Ru(ttp)(dppz)(4\text{-}PyCHAc)]^{2+}$ {[**1-Ac**]} was exposed to 470 nm LED light and the subsequent changes in the $^1$H NMR spectra in DMSO-$d_6$ were analyzed (Fig. 5). Upon gradual light irradiation, the peaks in the aliphatic region at 4.98, 2.08, 2.71 and 2.67 ppm were downfield shifted to 5.02, 2.13, 2.74 and 2.70 ppm, respectively, which indicates the release of the aldol adduct of 4-Pyridinecarboxaldehyde (*i.e.*, 4-PyCHAc). These aforementioned protons would lie along the shielding cone of the *p*-tolyl terpyridine ligand, while the pyridine ligand was conjugated with the Ru(II) center. Hence, after the release of the pyridine-based monodentate ligand (4-PyCHAc), the chemical shifts of the respective protons were downfield-shifted. In contrast, the doublet at 5.69 ppm in the complex corresponding to the –O**H** proton was upfield-shifted after the photorelease of the ligand to 5.60 ppm. The changes in the aromatic region were also analyzed to characterize the Ru(II)-based photoproduct in solution. In the aromatic region, the initial doublets at 9.89 and 9.15 ppm gradually diminished with gradual light exposure along with the concomitant emergence of a doublet at 10.46 ppm. Apart from that, the gradual emergence of one singlet at 9.37 ppm integrated for two hydro-

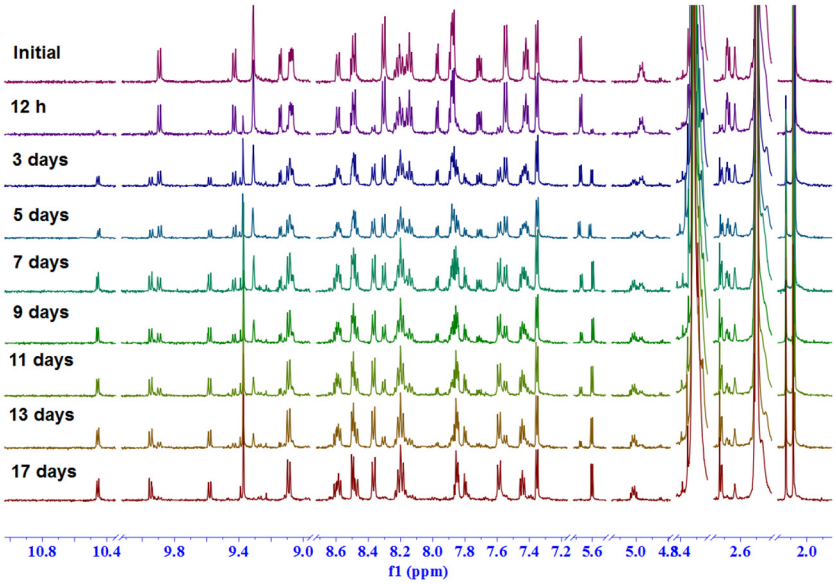


**Fig. 5** Time-dependent $^{1}$H NMR spectral change in DMSO-$d_6$, when [Ru(ttp)(dppz)(4-PyCHAc)]$^{2+}$ {[**1-Ac**]} was exposed to 470 nm blue LED light.

gens with simultaneous decay of the singlet at 9.31 ppm indicates one ruthenium-based photoproduct. Subsequent ESI-MS spectral analysis further corroborated the identity of the photoproduct as [Ru(ttp)(dppz)(DMSO-$d_6$)]$^{2+}$. The molecular ion peak at $m/z$ at 938.15 with a matching isotopic pattern can be ascribed to {[Ru(ttp)(dppz)(DMSO-$d_6$)]$^{2+}$ + 2[$NO_3^-$] + $Na^+$} (Fig. S8, ESI†). The identity of the released 4-PyCHAc ligand as an aldol adduct was also evidently established from the ESI-MS analysis of a peak with $m/z$ = 166.08. However, it is noteworthy to consider the exhaustive irradiation required for the photorelease of the pyridine-based 4-PyCHAc ligand from the Ru(II) center as is generally reported in the absence of sterically hindering bidentate ligands.[43] This, however, would not be practically applicable in actual *in vitro* and *in vivo* biological experiments to achieve the desirable photoindex (PI = $IC_{50}$ (dark)/$IC_{50}$ (light)). Therefore, for much more effective photorelease of the attached anticancer agents/drugs, sterically hindering bidentate ligands or nitrile/thioether based cageable moieties can be introduced in these systems.[2,3,32,43] The proposed photoreaction based on these experimental pieces of evidence is represented pictorially in Scheme 3.

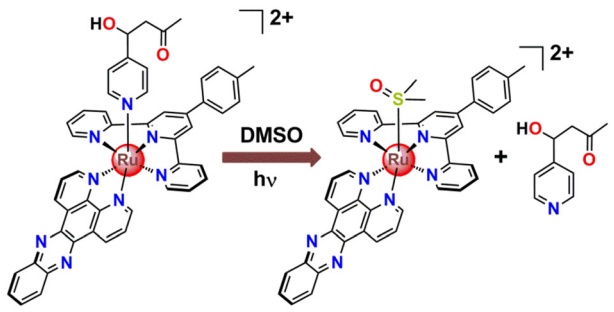


**Scheme 3** The photoinduced release of the pyridine-derived ligand from [Ru(ttp)(dppz)(4-PyCHAc)]$^{2+}$ {[**1-Ac**]}in DMSO under 470 nm LED light suggesting the release of the free ligand as the aldol adduct along with the formation of the {Ru-DMSO} adduct.

## Conclusion

This work focused on the thorough and unambiguous characterization of a serendipitous crossed aldol product, which resulted from the reaction of coordinated 4-Pyridinecarboxaldehyde (4-PyCHO) in the complex [Ru(ttp)(dppz)(4-PyCHO)]$^{2+}$ [**1**] and acetone while the complex was subjected to purification by silica gel column chromatography with acetone/water/saturated aqueous $KNO_3$ solution as the eluent. The original compound as [Ru(ttp)(dppz)(4-PyCHO)]$^{2+}$ was isolated after its synthesis as indicated by ESI-MS and $^{1}$H NMR and only underwent an aldol reaction during its purification. Subsequently, the pure product isolated from the column was characterized thoroughly in the solution state by $^{1}$H, $^{13}$C, $^{1}$H–$^{1}$H COSY and $^{1}$H–$^{13}$C HSQC NMR techniques as well as with ESI-MS as the aldol adduct [Ru(ttp)(dppz)(4-PyCHAc)]$^{2+}$ {[**1-Ac**]}. The identification of [**1-Ac**] was unequivocally determined in the solid state from its molecular structure by X-ray crystallography, which aligned with the observations in other spectroscopic techniques. Furthermore, the 4-PyCHAc ligand as an aldol product could be photoreleased from the Ru(II) center with blue LED light irradiation, and the subsequent speciation by ESI-MS studies established the identity of the photo-released ligand as the aldol adduct. Nonetheless, it should be mentioned that the less efficient photorelease of the ligand from the Ru(II)-caged system studied in this work would not be very effective for actual cytotoxic experiments. Therefore, improved design strategies are required to increase the efficiency of the photo-induced ligand substitution, which

 

would result in more effective delivery and/or release of cancer-targeting molecules attached to the cageable moiety. Despite that, this work portrays a proof-of-concept that provides an alternative synthetically handy strategy to attach uncageable cancer-targeting agents or other therapeutic loads to ruthenium(II) polypyridyl complexes for more selective and targeted anticancer chemotherapy.

# Experimental section

### Materials, methods and instrumentation

All the chemicals received from commercial sources were used in this work without further purification. The starting material $RuCl_3{\cdot}xH_2O$ was purchased from Sigma-Aldrich. 1,10-Phenanthroline, 4-Pyridinecarboxaldehyde and $KPF_6$ were purchased from Sigma-Aldrich. 2-Acetyl pyridine was purchased from Alfa Aesar. Lithium chloride and *p*-tolualdehyde were purchased from Avra Synthesis Pvt. Ltd. Triethyl ammine and silica gel (100–200 mesh size) for column chromatography were purchased from RANKEM Chemicals (Gurugram, India). The blue LED array light source (470 nm, LIU 470 A, 24 V, 15 W) used for photoreactivity studies was purchased from Thorlabs, USA. The deuterated solvents used for NMR characterization and photoreactivity studies were purchased from Sigma-Aldrich. Tetrabutylammonium hexafluorophosphate (TBAP) was used as a supporting electrolyte in cyclic voltammetry and was purchased from TCI Chemicals.

ESI-MS-based characterization studies were performed using a Q-TOF electrospray ionization mass spectrometer. UV-vis spectra were recorded using a JASCO-V670 spectrophotometer. Cyclic voltammetry was performed using a CH Instrument Model CHI 610 E potentiostat comprising a three-electrode cell system set-up, where glassy carbon (3 mm) was used as the working electrode, Ag/AgCl (0.1 M KCl) as the reference electrode and a Pt wire as the counter electrode. Ferrocene was added as an internal standard and the potentials were referenced against an $Fc^+/Fc$ couple. $^1$H NMR based characterization studies and the photoreactivity study were carried out using a JEOL ECX 500 spectrometer operating at 500 MHz. $^{13}$C NMR based characterization studies were performed by using an ECX 500 spectrometer operating at 125 MHz. The residual solvent peaks at 1.94 ppm ($CD_3CN$) and 4.79 ppm ($D_2O$) were used as references for $^1$H NMR chemical shifts. $^{13}$C NMR peaks were referenced with respect to the $CD_3CN$ residual signals at 1.32 and 118.26 ppm. Abbreviations for $^1$H NMR: s = singlet, d = doublet, t = triplet, m = multiplet, dd = doublet of doublets, and dt = doublet of triplets.

### X-ray crystallography

A suitable single crystal of [**1-Ac**] was mounted on a cryo-loop on a Bruker Apex-II CCD diffractometer. The source of the X-ray beam was Mo-κα ($\lambda$ = 0.71073 Å).[44] For indexing and determination of lattice parameters, the SMART program was used and the collection of the data was accomplished using a multi-scan technique, and the reduction and integration of the crude data were performed using the SAINT software package.[45] Absorption corrections were done using the SADABS program[46] and space group assignment was performed using SHELXTL. The crystal structure was solved by a direct method using the SHELXT program[47] in Olex2,[48] and least-squares full matrix refinement was performed using SHELXL[49] in Olex2. Anisotropic refinement was performed on all non-hydrogen atoms and the positions of the hydrogen atoms were determined from the electron density map. The refinement details and crystallographic parameters for [**1-Ac**] are given in Table S3 in the ESI.† The perspective image of the molecular structure shown in Fig. 4 was generated from Mercury 4.2.0.

### Synthesis

The syntheses of the *p*-tolyl terpyridine (ttp) and dppz = dipyrido[3,2-*a*:2′,3′-*c*]phenazine (dppz) ligands, as well as $[Ru(ttp)(Cl)_3]$, $[Ru(ttp)(dppz)(Cl)](PF_6)$, and $[Ru(ttp)(dppz)(H_2O)](PF_6)_2$, were done by adopting similar methods as described in the literature reports.[40–42,50,51]

**$[Ru(ttp)(dppz)(4\text{-}PyCHO)]^{2+}$ {[1]} and $[Ru(ttp)(dppz)(4\text{-}PyCHAc)]^{2+}$ {[1-Ac]}.** 200 mg (0.19 mmol) of $[Ru(ttp)(dppz)(H_2O)](PF_6)_2$ was dissolved in 50 mL of acetone and 54 μL of 4-pyridine carboxaldehyde (0.57 mmol) was added and refluxed for 24 h under a nitrogen atmosphere. After 24 h, the solvent was evaporated using a rotary evaporator and a dark red compound was isolated. ESI-MS in MeOH (+): *m*/*z* (calculated): 991.16, (experimental): 991.16 $[M - PF_6^-]^+$. Thereafter, the complex was subjected to purification using a silica column and eluted with acetone/water/saturated aqueous $KNO_3$ solution (85 : 5 : 0.5) as the eluent. $^1$H NMR {500 MHz, $(CD_3)_2SO$} $\delta$ 9.89 (d, $J$ = 8.2 Hz, 1H), 9.43 (d, $J$ = 8.1 Hz, 1H), 9.31 (s, 2H), 9.15 (d, $J$ = 5.5 Hz, 1H), 9.08 (dd, $J$ = 8.3, 3.9 Hz, 2H), 8.61–8.57 (m, 1H), 8.50 (dd, $J$ = 8.1, 5.5 Hz, 2H), 8.31 (d, $J$ = 8.2 Hz, 2H), 8.24–8.17 (m, 2H), 8.15 (t, $J$ = 7.8 Hz, 2H), 7.98 (d, $J$ = 5.5 Hz, 1H), 7.91–7.86 (m, 4H), 7.71 (dd, $J$ = 8.3, 5.4 Hz, 1H), 7.55 (d, $J$ = 8.1 Hz, 2H), 7.44–7.40 (m, 2H), 7.36 (d, $J$ = 6.5 Hz, 2H), 5.69 (d, $J$ = 5.1 Hz, 1H), 4.98 (X-part of the ABX pattern, 1H), 2.71 and 2.67 (AB part of the ABX pattern, 2H), 2.08 (s, 3H).$^{13}$C NMR {125 MHz, $(CD_3)_2SO$} $\delta$ 206.5, 158.4, 157.8, 157.0, 153.9, 153.7, 152.0, 151.0, 150.2, 147.9, 142.5, 142.4, 141.0, 140.8, 140.4, 139.1, 133.4, 133.3, 133.1, 133.0, 132.9, 130.8, 130.5, 129.9, 129.8, 129.1, 128.2, 128.1, 127.3, 125.8, 124.1, 121.4, 67.2, 51.6, 30.7, 21.5. ESI-MS in MeOH (+): *m*/*z* (calculated): 934.20, (experimental): 934.20 $[M - NO_3^-]^+$.

# Author contributions

Ramranjan Mishra: conceptualization, purification, characterization, photoreactivity study, data analysis, validation and manuscript writing. Pritha Chatterjee: synthesis, characterization and purification. Ray J. Butcher: solving the crystal structure. Ashis K. Patra: reviewing and editing the manuscript, project administration, funding acquisition, and supervision.

## Data availability

The data supporting this article have been included as part of the ESI.† Crystallographic data for [**1-Ac**] in CIF format have been deposited at the CCDC (2377849).†

## Conflicts of interest

There are no conflicts to declare.

## Acknowledgements

The authors gratefully acknowledge the Indian Council of Medical Research (ICMR) (project no. 2020-2677) and the Council of Scientific and Industrial Research (CSIR) (project no. 01(3048)/21/EMR-II) for financial support. R. M. thanks CSIR and P. C. acknowledges the Department of Science and Technology (DST) for the respective research fellowships.

## References

1 L. Conti, E. Macedi, C. Giorgi, B. Valtancoli and V. Fusi, *Coord. Chem. Rev.*, 2022, **469**, 214656.
2 S. Bonnet, *J. Am. Chem. Soc.*, 2023, **145**, 23397–23415.
3 S. Bonnet, *Dalton Trans.*, 2018, **47**, 10330–10343.
4 D. Havrylyuk, K. Stevens, S. Parkin and E. C. Glazer, *Inorg. Chem.*, 2020, **59**, 1006–1013.
5 S. Bonnet, B. Limburg, J. D. Meeldijk, R. J. M. K. Gebbink and J. A. Killian, *J. Am. Chem. Soc.*, 2011, **133**, 252–261.
6 A. Bahreman, J.-A. Cuello-Garibo and S. Bonnet, *Dalton Trans.*, 2014, **43**, 4494–4505.
7 V. H. S. van Rixel, B. Siewert, S. L. Hopkins, S. H. C. Askes, A. Busemann, M. A. Siegler and S. Bonnet, *Chem. Sci.*, 2016, **7**, 4922–4929.
8 R. E. Goldbach, I. Rodriguez-Garcia, J. H. van Lenthe, M. A. Siegler and S. Bonnet, *Chem. – Eur. J.*, 2011, **17**, 9924–9929.
9 T. N. Rohrabaugh Jr, K. A. Collins, C. Xue, J. K. White, J. J. Kodanko and C. Turro, *Dalton Trans.*, 2018, **47**, 11851–11858.
10 S. J. Steinke, E. J. Piechota, L. M. Loftus and C. Turro, *J. Am. Chem. Soc.*, 2022, **144**, 20177–20182.
11 A. P. Lanquist, S. Gupta, K. F. Al-Afyouni, M. Al-Afyouni, J. J. Kodanko and C. Turro, *Chem. Sci.*, 2021, **12**, 12056–12067.
12 L. M. Loftus, K. F. Al-Afyouni, T. N. Rohrabaugh, J. C. Gallucci, C. E. Moore, J. J. Rack and C. Turro, *J. Phys. Chem. C*, 2019, **123**, 10291–10299.
13 M. A. Sgambellone, A. David, R. N. Garner, K. R. Dunbar and C. Turro, *J. Am. Chem. Soc.*, 2013, **135**, 11274–11282.
14 D. Unjaroen, J. Chen, E. Otten and W. R. Browne, *Inorg. Chem.*, 2017, **56**, 900–907.
15 D. E. S. Silva, M. P. Cali, W. M. Pazin, E. Carlos-Lima, M. T. S. Trevisan, T. Venâncio, M. Arcisio-Miranda, A. S. Ito and R. M. Carlos, *J. Med. Chem.*, 2016, **59**, 9215–9227.
16 J. D. Knoll, B. A. Albani and C. Turro, *Chem. Commun.*, 2015, **51**, 8777–8780.
17 L. M. Loftus, J. K. White, B. A. Albani, L. Kohler, J. J. Kodanko, R. P. Thummel, K. R. Dunbar and C. Turro, *Chem. – Eur. J.*, 2016, **22**, 3704–3708.
18 T. N. Rohrabaugh, A. M. Rohrabaugh, J. J. Kodanko, J. K. White and C. Turro, *Chem. Commun.*, 2018, **54**, 5193–5196.
19 L. Zayat, M. Salierno and R. Etchenique, *Inorg. Chem.*, 2006, **45**, 1728–1731.
20 R. Cabrera, O. Filevich, B. García-Acosta, J. Athilingam, K. J. Bender, K. E. Poskanzer and R. Etchenique, *ACS Chem. Neurosci.*, 2017, **8**, 1036–1042.
21 N. Karaoun and A. K. Renfrew, *Chem. Commun.*, 2015, **51**, 14038–14041.
22 H. Chan, J. B. Ghrayche, J. Wei and A. K. Renfrew, *Eur. J. Inorg. Chem.*, 2017, **12**, 1679–1686.
23 C. R. Cardoso, I. de Aguiar, M. R. Camilo, M. V. S. Lima, A. S. Ito, M. S. Baptista, C. Pavani, T. Venâncio and R. M. Carlos, *Dalton Trans.*, 2012, **41**, 6726–6734.
24 M. Hirahara and Y. Umemura, *Inorg. Chem.*, 2021, **60**, 13193–13199.
25 P. A. Scattergood, U. Khushnood, A. Tariq, D. J. Cooke, C. R. Rice and P. I. P. Elliott, *Inorg. Chem.*, 2016, **55**, 7787–7796.
26 C. E. Welby, S. Grkinic, A. Zahid, B. S. Uppal, E. A. Gibson, C. R. Rice and P. I. P. Elliott, *Dalton Trans.*, 2012, **41**, 7637–7646.
27 D. Havrylyuk, M. Deshpande, S. Parkin and E. C. Glazer, *Chem. Commun.*, 2018, **54**, 12487–12490.
28 F. J. Ballester, A. Hernández-Garcia, M. D. Santana, D. Bautista, P. Ashoo, E. Ortega-Forte, G. Barone and J. Ruiz, *Inorg. Chem.*, 2024, **63**, 6202–6216.
29 G. E. Giacomazzo, L. Conti, C. Fagorzi, M. Pagliai, C. Andreini, A. Guerri, B. Perito, A. Mengoni, B. Valtancoli and C. Giorgi, *Inorg. Chem.*, 2023, **62**, 7716–7727.
30 M. Huisman, J. K. White, V. G. Lewalski, I. Podgorski, C. Turro and J. J. Kodanko, *Chem. Commun.*, 2016, **52**, 12590–12593.
31 K. Arora, M. Herroon, M. H. Al-Afyouni, N. P. Toupin, T. N. Rohrabaugh Jr., L. M. Loftus, I. Podgorski, C. Turro and J. J. Kodanko, *J. Am. Chem. Soc.*, 2018, **140**, 14367–14380.
32 M. Denison, S. P. Garcia, A. Ullrich, I. Podgorski, H. Gibson, C. Turro and J. J. Kodanko, *Inorg. Chem.*, 2024, **63**, 7973–7983.
33 S. Marrache and S. Dhar, *Chem. Sci.*, 2015, **6**, 1832–1845.
34 P. L. J. Pedersen, *Bioenerg. Biomembr.*, 2012, **44**, 1–6.
35 Z. Liu, Y. Sun, H. Hong, S. Zhao, X. Zou, R. Ma, C. Jiang, Z. Wang, H. Li and H. Liu, *Am. J. Cancer Res.*, 2015, **5**, 2673–2685.
36 B. J. Coe, J. Fielden, S. P. Foxon, B. S. Brunschwig, I. Asselberghs, K. Clays, A. Samoc and M. Samoc, *J. Am. Chem. Soc.*, 2010, **132**, 3496–3513.

 

37 D. Chao and W.-F. Fu, *Chem. Commun.*, 2013, **49**, 3872–3874.
38 S. Gouthaman, S. Periyaraja and P. Shanmugam, *Tetrahedron Lett.*, 2015, **56**, 5920–5923.
39 J. Karges, F. Heinemann, F. Maschietto, M. Patra, O. Blacque, I. Ciofini, B. Spingler and G. Gasser, *Bioorg. Med. Chem.*, 2019, **27**, 2666–2675.
40 S. Bonnet, J.-P. Collin, N. Gruber, J.-P. Sauvage and E. R. Schofield, *Dalton Trans.*, 2003, **24**, 4654–4662.
41 Q.-X. Zhou, F. Yang, W.-H. Lei, J.-R. Chen, C. Li, Y.-J. Hou, X.-C. Ai, J.-P. Zhang, X.-S. Wang and B.-W. Zhang, *J. Phys. Chem. B*, 2009, **113**, 11521–11526.
42 R. Mishra, A. Saha, P. Chatterjee, A. Bhattacharyya and A. K. Patra, *Inorg. Chem.*, 2023, **62**, 18839–18855.
43 J. D. Knoll, B. A. Albani, C. B. Durr and C. Turro, *J. Phys. Chem. A*, 2014, **118**, 10603–10610.
44 *APEX2 V2012.4*, Bruker AXS Inc., Madison, USA, 2012.
45 *SMART & SAINT Software Reference manuals, Version 6.45*, Bruker Analytical X-ray Systems, Inc., Madison, WI, 2003.
46 G. M. Sheldrick, *SADABS, Software for empirical absorption correction, Ver. 2.05*, University of Göttingen, Göttingen, Germany, 2002.
47 G. M. Sheldrick, SHELXT – Integrated space-group and crystal structure determination, *Acta Crystallogr., Sect. A: Found. Adv.*, 2015, **71**, 3–8.
48 O. V. Dolomanov, L. J. Bourhis, R. J. Gildea, J. A. K. Howard and H. J. Puschmann, *OLEX2*: a complete structure solution, refinement and analysis program, *J. Appl. Crystallogr.*, 2009, **42**, 339–341.
49 G. M. Sheldrick, Crystal structure refinement with SHELXL, *Acta Crystallogr., Sect. C: Struct. Chem.*, 2015, **71**, 3–8.
50 Y. Chen, W. Guo, Z. Ye, G. Wang and J. Yuan, *Chem. Commun.*, 2011, **47**, 6266–6268.
51 M. S. Deshpande, A. S. Kumbhar and C. Näther, *Dalton Trans.*, 2010, **39**, 9146–9152.